



Resistance of Flat-Plate Buildings against Progressive Collapse. I: Modeling of Slab-Column Connections

Jinrong Liu¹; Ying Tian, M.ASCE²; Sarah L. Orton, M.ASCE³; and Aly M. Said, M.ASCE⁴

Abstract: A macromodel for slab-column connections is created for use in the system-level progressive collapse analyses of reinforced concrete flat-plate structures. The proposed model jointly uses shell and connector elements to simulate the complex behavior of slabs. Shell elements are used to simulate the flexural response of slab and the load redistribution over floor slabs. The connector elements, which permit simulating separation of slab from column on a punching failure, are defined with nonlinear responses for primary bending moment and torsion. A deformation-based punching failure criterion is defined for connector elements to simulate the punching failure at a slab-column connection and failure propagation. Parameters defining concrete tension stiffening behavior under static loading, including the peak tensile stress and the tensile strain when stress degrades to zero, are calibrated from two experiments. To ensure applicability, the proposed model is validated by 24 large-scale tests conducted on isolated slab-column connection specimens subjected to concentric gravity loading, torsional loading, and uneven gravity loading. DOI: [10.1061/\(ASCE\)ST.1943-541X.0001294](https://doi.org/10.1061/(ASCE)ST.1943-541X.0001294). © 2015 American Society of Civil Engineers.

Author keywords: Flat plate; Flat slab; Slab-column connection; Punching shear; Shell element; Progressive collapse; Analysis and computation.

Introduction

Reinforced concrete flat-plate structures consist of slabs with uniform thickness supported directly on columns. Flat plate is a major class of structural system popularly used for commercial and residential buildings because of its simple formwork, lower construction cost, larger clear space, and architectural flexibility. Despite these advantages, a flat plate is prone to punching failure of slabs caused by the highly concentrated shear and moment at the vicinity of columns. When punching failure occurs at a slab-column connection, the gravity load initially carried by this connection is redistributed to the neighboring connections, which may cause further punching failures in these locations and failure propagation over the floor slab. If the floor slab cannot develop an adequate tensile membrane action to carry gravity loads, a progressive collapse of the building may result. Of particular concern is the collapse resistance of older flat-plate buildings. There is a large inventory of flat plates in the United States designed on the basis of the pre-1989 American Concrete Institute (ACI) codes. These flat plates, lacking of both slab shear reinforcement and continuous bottom bars

through the columns as structural integrity reinforcement, have little capability to develop a tensile membrane action in slabs and, therefore, are highly vulnerable to progressive collapse.

The robustness of a flat-plate structure against progressive collapse, as recommended by the Department of Defense (DoD 2009) guideline, can be assessed by notionally removing a load-bearing column instantaneously. The column removal causes a complex loading condition at the neighboring slab-column connections. Given that slabs are primary load-carrying components in a flat-plate structure, an effective analysis tool is needed to capture the prepunching behavior of slabs, punching failure at slab-column connections, and failure propagation. In addition, simulating the performance of an entire structural system calls for reduced modeling approaches, such as those proposed by Bao et al. (2008) for reinforced concrete moment frames and Khabdekwal et al. (2008) for steel moment frames.

The existing equivalent frame and equivalent beam methods (Morrison et al. 1983; Akiyama and Hawkins 1984; Luo et al. 1995; Robertson 1997; Tian et al. 2009; Kang et al. 2009), as simplified modeling approaches, were calibrated for flat plates dominated by seismic lateral loading. Moreover, both methods are two dimensional (2D) in nature because a spatially continuous flat-plate system needs to be idealized into planar frames, thereby having limited capability of capturing load redistribution over floor slabs in the column removal scenario. Grid model (Sheu and Hawkins 1980; Coronelli 2010; Tian et al. 2012) simulates slabs by crossing beam elements. This model requires more modeling efforts but has potential to be applied to the progressive collapse analyses of flat plates if the effects of slab membrane actions on load-carrying capacity can be incorporated.

Using shell elements to model flat plates involves moderate computational efforts and was investigated by some studies (Marzouk and Chen 1993; Loo and Guan 1997; Polak 1998; Wang and Teng 2008) on the basis of various formulations. The goal of this study is to develop a macro-finite-element (FE) model using both shell and connector elements to simulate the nonlinear response and the ultimate punching failure of slab-column connections subjected to complex loading conditions. The macromodel

¹Structural Engineer, Mendenhall Smith Structural Engineers, Las Vegas, NV 89117; formerly, Ph.D. Student, Univ. of Nevada, 4505 S. Maryland Parkway, Las Vegas, NV 89154. E-mail: JLiu@mendenhallsmith.com

²Associate Professor, Dept. of Civil and Environmental Engineering and Construction, Univ. of Nevada, 4505 S. Maryland Parkway, Las Vegas, NV 89154 (corresponding author). E-mail: ying.tian@unlv.edu

³Associate Professor, Dept. of Civil and Environmental Engineering, Univ. of Missouri-Columbia, Columbia, MO 65211. E-mail: ortons@missouri.edu

⁴Associate Professor, Dept. of Architectural Engineering, Pennsylvania State Univ., 104 Engineering Unit A, University Park, PA 16802; formerly, Associate Professor, Dept. of Civil Engineering and Construction, Univ. of Nevada, 4505 S. Maryland Parkway, Las Vegas, NV 89154. E-mail: aly.said@enr.psu.edu

Note. This manuscript was submitted on May 27, 2014; approved on January 26, 2015; published online on March 18, 2015. Discussion period open until August 18, 2015; separate discussions must be submitted for individual papers. This paper is part of the *Journal of Structural Engineering*, © ASCE, ISSN 0733-9445/04015053(13)/\$25.00.

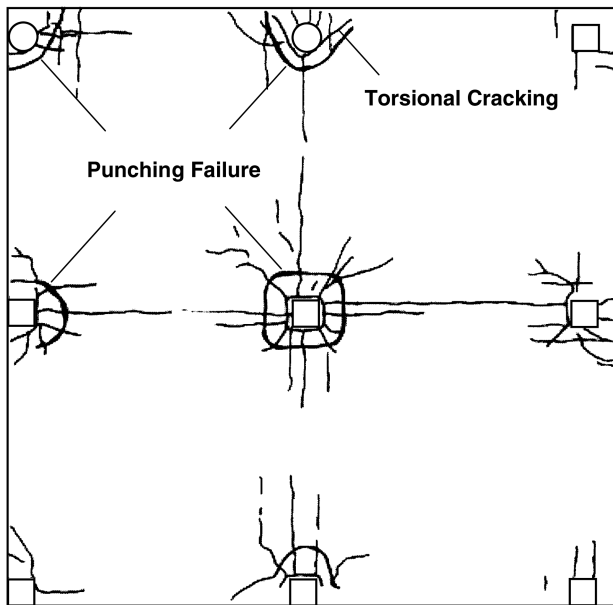


Fig. 1. Damage pattern of a continuous flat-plate specimen (Gardner and Shao 1996, reproduced with permission from the American Concrete Institute)

will be applied in the progressive collapse analyses of older flat-plate buildings presented in a companion paper.

Insights from Experiments

Experiment results are instructive for creating a behavioral model for flat plates. Multipanel tests (Gardner and Shao 1996) indicated that damage caused by concrete cracking and slab yielding (Fig. 1) was concentrated in the slab near the columns, indicating the importance of modeling the nonlinear behavior of slab-column connections. Punching is typically the ultimate failure mode of flat plates; however, punching is not purely a shear problem. Experiments (Elstner and Hognestad 1956; Moe 1961; Criswell 1974; Guandalini et al. 2009; Tian et al. 2008b) have repeatedly indicated that the failure mode of a slab-column connection depends on slab flexural reinforcement ratio, which affects the extent of yielding, ultimate strength, and deformation capacity. In general, the response of slab-column connections with low slab reinforcement ratios is controlled by flexure, and punching failure occurs only after large nonlinear deformation; for slabs with moderate reinforcement ratios, flexural yielding still occurs in slab near the column, but the connections have limited ductility. These observations highlight the significance of slab flexural behavior, which can be modeled by using shell elements if nonlinear material properties are properly defined.

Additionally, unbalanced moment transferred between slab and column, if any, causes torsion. Torsional cracks can be clearly seen in Fig. 1 at the exterior slab-column connections where unbalanced moment existed. Given that torsion affects the distribution of internal forces in slab among different column sides, torsional stiffness and strength must be rationally modeled. Finally, the material property of concrete is not homogeneous. Fig. 2 (Tian 2007) shows a slab-column connection failed by punching attributed to concentric gravity loading. The marked cracks caused by slab bending were observed well before the final punching failure. Because of coarse aggregate settlement, the concrete situated above the slab top reinforcement was weaker, leading to concrete cracking along these bars before punching failure in some tests. This property can also be

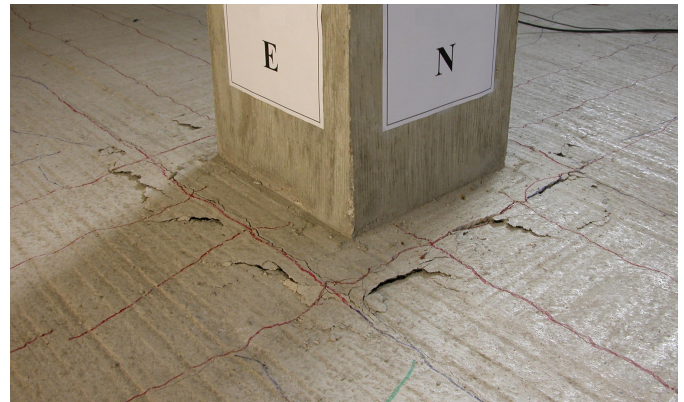


Fig. 2. Cracking and punching failure of a slab-column connection tested under concentric gravity loading (reprinted from Tian 2007)

seen in Fig. 1. The inclined cracks leading to punching failure are initiated along a slab top bar parallel to column face, as shown in Fig. 2.

Overview of Proposed Macromodel

The FE package *ABAQUS* (2010) is adopted as modeling platform. The proposed macromodel, shown in Fig. 3, jointly uses shell and connector elements. The shell elements are used to simulate the flexural response of slabs and load redistribution over the entire floor slab. The connector elements are used to model the internal force transfer between slab and column and the punching failure of slab. Consistent with the ACI 318-11 (ACI 2011) provisions, a punching perimeter (critical section) is assumed to be located at a distance of half the slab effective depth ($d/2$) away from column faces. The slab-column joint area is modeled by rigid shell elements. Because the thickness of a floor slab is significantly smaller than its two other dimensions, the slab outside the critical section is modeled by shell elements defined with rebar layers and nonlinear material properties. The use of shell elements permits effectively simulating the effects of compressive and tensile membrane actions.

The slab encompassed by the assumed punching perimeter but outside the slab-column joint is idealized as a series of short beams

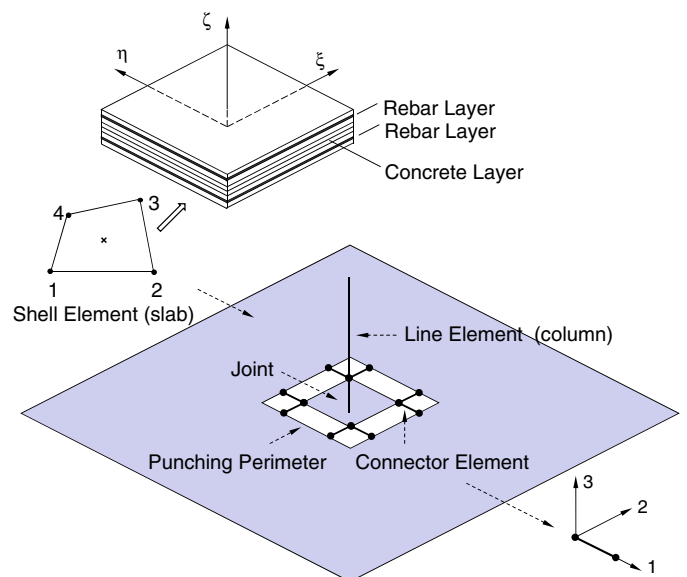


Fig. 3. Schematic of proposed macromodel for flat plate

modeled with connector elements. Cartesian-Cardan connectors with six degrees of freedom are adopted. For convenience, these beams are termed as connector beams in the following discussions. Two connector beams are used at each side of a slab-column joint and oriented perpendicular to column face. Each connector beam is rigidly connected with the joint at one end by sharing all degrees of freedom and connected with a node of shell elements for slab at another end. Before a punching failure, all degrees of freedom at this node are shared by the connector beam and the shell elements so that bending moment, shear, and torsion are transferred from slab to column. Each connector beam is assumed with a length of $d/2$, a depth of h , and a width of $b = 0.5(c + d)$, where h is slab thickness, and c is column width. The torsion and axial force transferred by a connector beam rely on the relative twist angle and relative axial displacement between the two nodes, respectively. Because of the very short length of a connection beam (less than half the slab thickness and less than 1.5% of the span length of a typical flat-plate structure), bending moment is assumed as constant along the beam and depends only on the relative rotation of connector ends. Similarly, shear is taken as only a function of relative transverse displacement between the two nodes. Thus, the connector beams are assigned with uncoupled behaviors for flexure, shear, axial force, and torsion.

Because shell elements are difficult to use in shear failure simulation, a punching failure criterion is defined for the connector beams. No postpunching resistance is assumed for the connector beams because of the following reasons: Following a punching failure in slab and after the inclined cracks are widened enough to completely penetrate the slab, concrete interlocking force disappears and there is a transition in slab from dowel action to tensile membrane action to resist gravity loads. Without using appropriate type of slab shear reinforcement, such as stirrups, the top bars cannot be restrained from being stripped out of slab because of the propagation of concrete cover spalling on a punching failure. Thus, the development of either dowel or tensile membrane action relies on slab bottom bars. However, in older flat-plate buildings, the slab bottom bars are anchored into the column with neither continuity nor sufficient development length. They will be pulled out of column and therefore cannot be engaged to develop an effective tensile membrane action. Accordingly, once the failure condition is met in the macromodel, the connector beams will be automatically separated from the slab by eliminating the sharing of degrees of freedom at nodes and no longer effective to resist any load. Although the proposed macromodel is developed for older flat-plate constructions, it can also be used to simulate the prepunching behavior of flat plates having structural integrity reinforcement. Moreover, by adding other types of connector elements, the model can be extended to simulate the postpunching resistance provided by slab tensile membrane action.

Modeling Slabs with Shell Elements

Material Properties

Slab flexural reinforcement is modeled as uniaxial material. A bilinear stress-strain response is assumed by specifying yield stress, yield strain, and a 1% strain hardening ratio unless the postyielding behavior is known. According to their area, spacing, location, and orientation, the slab top and bottom reinforcement are defined as rebar layers in the shell elements. Concrete damage plasticity (Lubliner et al. 1989; Lee and Fenves 1998) is adopted to define the concrete constitutive relationship under a triaxial state of stress. This concrete material model is suitable for rate-sensitive analyses, such as dynamic progressive collapse analyses, and can be applied to not only implicit algorithm but also explicit algorithm. The concrete

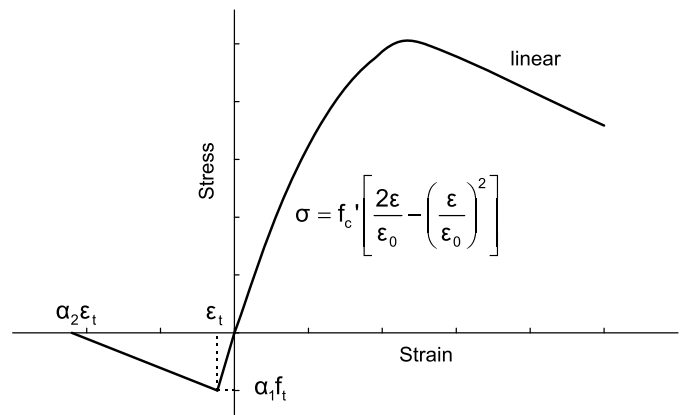


Fig. 4. Uniaxial stress-strain relationship considered for concrete in the shell elements

damage plasticity uses the Drucker-Prager-type yield function, considers nonassociated flow rule, and incorporates a set of damage parameters to represent stiffness degradation along with plastic deformations. Because no transverse reinforcement is used in the slab, the dilation angle is defined as 30° on the basis of the recommendations made by Mercan et al. (2010) for lightly-to-moderately confined concrete. The ratio of initial equibiaxial compressive yield stress to initial uniaxial compressive yield stress is defined as 1.16. The ratio of the second stress invariant on the tensile meridian to that on the compressive meridian is defined as 0.667.

To implement the concrete damage plasticity model, the uniaxial behavior of concrete needs to be specified. Concrete Young's modulus is defined according to ACI 318-11 (ACI 2011). The stress-strain relationship suggested by Hognestad (1951), as shown in Fig. 4, is adopted to define the uniaxial behavior of concrete in compression and tension. Concrete tensile behavior greatly affects slab flexural stiffness, membrane action, and convergence of a numerical analysis. A bilinear response, as shown in Fig. 4, is adopted for concrete in tension. To account for the initial tensile stress caused by restrained concrete shrinkage before applying any loads and the reduced concrete tensile strength caused by coarse aggregate settlement, the peak concrete tensile stress is defined as $\alpha_1 f_t$, where f_t is concrete tensile strength according to ACI 318-11 (ACI 2011). Concrete tension stiffening, which is more pronounced in lightly reinforced concrete members (Massicotte et al. 1990) such as typical floor slabs, is defined by a linear descending branch through parameter α_2 , the ratio of strain when stress degrades to zero to the strain at peak stress. The appropriate values of α_1 and α_2 are calibrated from static loading tests, as discussed subsequently. Because of the lack of relevant test data, it is assumed that, although concrete tensile strength increases under higher strain rates, the calibrated α_1 and α_2 are still applicable. Shear stiffness degradation is not considered for concrete, and its Poisson's ratio is defined as 0.2.

Choice of Shell Element Type

According to sensitivity analyses, the maximum mesh size for the shell elements used in this study is chosen to be less than the slab thickness. Four-node thin shell elements with reduced integration, rather than thick shell elements, are used because the use of shell elements in this study is intended to simulate the slab outside the punching failure region, where the response is dominated by flexure. Even though thick shell takes into account the transverse shear deformation, such a deformation in slab-column connections without slab shear reinforcement before punching failure is small (Lips et al. 2012). In addition, thick shell elements can only be used

Table 1. Geometric and Material Properties of Simulated Specimen

Loading condition	Reference	Specimen	Slab dimension (mm)	Column size (mm)	Concrete strength (MPa)	Steel yield strength (MPa)	Slab tensile reinforcement ratio (%)
Concentric gravity loading	Elstner and Hognestad (1956)	A-1c	1,829 × 1,829 × 154	254	29.0	332	1.15
		A-4	1,829 × 1,829 × 154	356	26.1	332	1.15
		A-13	1,829 × 1,829 × 154	356	26.2	294	0.55
		B-1	1,829 × 1,829 × 154	254	14.2	324	0.50
		B-2	1,829 × 1,829 × 154	254	47.6	321	0.50
		B-4	1,829 × 1,829 × 154	254	47.7	303	0.99
	Broms (2000)	9a	2,600 × 2,600 × 180	250	21.0	510	0.50
		Guandalini et al. (2009)	PG-2 b	3,000 × 3,000 × 250	260	40.5	552
	This study ^a	PG-5	3,000 × 3,000 × 250	260	29.3	555	0.33
		PG-11	3,000 × 3,000 × 250	260	31.5	570	0.75
		1.0UN	1,770 × 1,770 × 140	279	33.4	428	1.00
		0.64UN	1,770 × 1,770 × 140	279	32.4	428	0.67
		1.0RE	1,770 × 1,770 × 140	279	36.4	428	1.00
Torsion	Kano and Yoshizaki (1979)	0.64RE-NH2	1,770 × 1,770 × 140	279	37.0	428	0.67
		T-2	2,000 × 800 × 100	200	25.7	377	0.98
		T-3	2,000 × 800 × 100	200	25.7	377	2.00
		T-7	2,000 × 600 × 100	200	25.7	377	0.98
		T-8	2,000 × 400 × 100	200	25.7	377	0.98
Uneven gravity loading	Hawkins et al. (1989)	6AH	2,134 × 2,134 × 154	305	31.4	472	0.60
		6AL	2,134 × 2,134 × 154	305	22.8	472	0.60
		9.6AH	2,134 × 2,134 × 154	305	30.7	415	0.96
		9.6AL	2,134 × 2,134 × 154	305	29.0	415	0.96
		14AH	2,134 × 2,134 × 154	305	30.3	421	1.40
		14AL	2,134 × 2,134 × 154	305	27.0	421	1.40

^aWithout continuous slab bottom reinforcement at columns.

for small strain because thick shell elements are subjected to shear locking when a structural component is thin (Cook et al. 2001). Thick shells can also cause rank deficiency and lead to singularity of global stiffness matrix (Parisich 1979).

The applications of four-node thin and eight-node thick shell elements to slab-column connections are compared by simulating the experiments of two isolated slab-column specimens, B-2 and B-4, tested by Elstner and Hognestad (1956) under concentric gravity loading. These specimens had almost the same material strength but different reinforcement ratios. The properties of these specimens and others used for model calibration and validation purposes are given in Table 1. To eliminate the effects of using connector elements, the slabs of the specimens are modeled only by shell elements. Fig. 5 shows the simulated load-center deflection responses against test data, indicating that the predicted responses using thin and thick elements are almost identical before slab yielding and negligible difference exists for postyielding response.

Modeling Connector Beams

Flexural Behavior

Because of the high rigidity of the column, bending moment in the slab immediately outside the column exists mainly about a horizontal axis parallel to the column face. A trilinear moment-curvature relationship, as shown in Fig. 6(a) is assigned to the primary bending moment denoted in this paper as M to account for slab cracking, yielding, and reaching ultimate strength. The moment at cracking M_{cr} , curvature at cracking ϕ_{cr} , moment at yielding M_y , curvature at yielding ϕ_y , ultimate moment M_u , and ultimate curvature ϕ_u are computed on the basis of the assumed dimension of a connector beam and the conventional approach for a reinforced concrete beam. Because of the confinement effect provided by the surrounding slab, a concrete compressive strain of 0.004 is used to define the

ultimate state. Because concrete crushing generally cannot be observed in the test of a slab-column connection before its punching failure, defining the ultimate moment and curvature by using the assumed ultimate strain of concrete in compression (0.004) is used mainly to control postyielding flexural stiffness. To consider axial force-flexure interaction for slabs having in-plane restraints, an analysis can be performed first without considering this interaction. From the analysis results, the in-plane force intensity in the shell elements outside the connector beams are obtained and used to determine axial force in these connector elements, from which M_y , ϕ_y , M_u , and ϕ_u can be redefined to improve analysis results. The constitutive model for primary bending is given by using an incremental format as

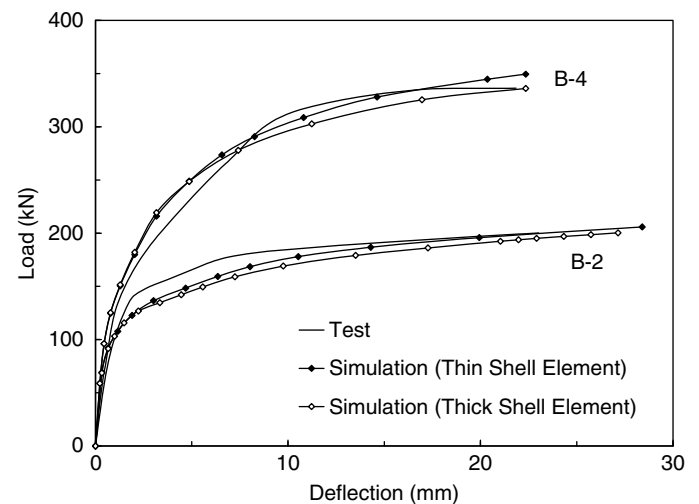


Fig. 5. Comparison between using thin and thick shell elements to simulate slab-column connections tested by Elstner and Hognestad (1956)

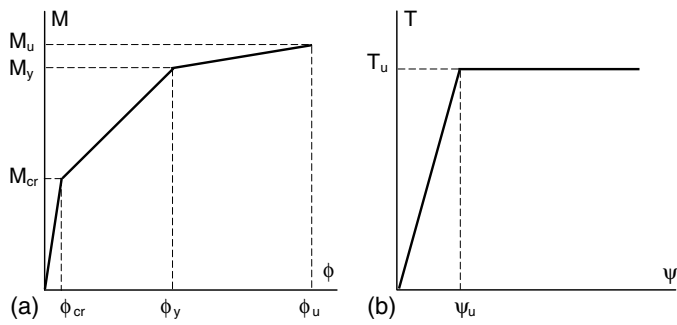


Fig. 6. Nonlinear sectional behavior models for connector beams: (a) flexure; (b) torsion

$$\Delta M = K_M \Delta \theta = \Delta \theta \cdot \begin{cases} \frac{M_{cr}}{\phi_{cr} L} & (0 \leq \theta_2 \leq \phi_{cr} L) \\ \frac{M_y - M_{cr}}{(\phi_y - \phi_{cr}) L} & (\phi_{cr} L < \theta_2 \leq \phi_y L) \\ \frac{M_u - M_y}{(\phi_u - \phi_y) L} & (\phi_y L < \theta_2 \leq \phi_u L) \end{cases} \quad (1)$$

where K_M = flexural rigidity of connector beam; θ_2 = relative rotation angle about local Axis 2 between the two nodes of a connector beam shown in Fig. 3; and L = length of connector beam.

The connector beams are also assigned with flexural behavior about the vertical axis (Axis 3 in Fig. 3). However, this in-plane bending moment is assumed as linear elastic with a very high flexural stiffness to account for the effects of continuity actually existing in a slab.

Torsional Behavior

The tests conducted by Kanoh and Yoshizaki (1979) on slab-column connections subjected to externally applied torque revealed that slab longitudinal reinforcement had little effect on torsional resistance. In addition, Hsu (1968b) found that the increase in torsional strength of reinforced concrete beams caused by longitudinal bars rarely exceeded 15% and that this contribution was unreliable. Therefore, the torsional strength T_u of a connector beam is assumed only as a function of concrete strength and section geometry. T_u and the corresponding twist angle ψ_u (in rad/mm) are defined by Eqs. (2) and (3) on the basis of the formulations derived from the tests of plain concrete beams (Hsu 1968a)

$$T_{cr} = 0.217y(x^2 + 6450)(\sqrt[3]{f'_c}) \text{ (in mm and MPa)} \quad (2)$$

$$\psi_u = \frac{4.36 \times 10^{-4}}{\sqrt{xy}} \left(1 + \frac{6450}{x^2} \right) \text{ (in mm)} \quad (3)$$

where x and y = dimension of short and long sides of the beam cross section, respectively; and f'_c = concrete compressive strength.

From these tests, ψ_u was found not affected by material property. It was also observed from the torsional tests of slab-column connections (Kanoh and Yoshizaki 1979) that, because of the existence of flexural reinforcement, torsional cracking of slab near the column did not lead to an immediate drop of torsional strength, and the torsional behavior was fairly ductile. Therefore, an elastic-perfectly plastic response, as shown in Fig. 6(b), is assumed for torsion in the connector beams. The incremental constitutive function for torsion is defined as

$$\Delta T = K_T \Delta \theta_1 = \Delta \theta_1 \cdot \begin{cases} \frac{T_{cr}}{\psi_u L} & (0 \leq \theta_1 \leq \psi_u L) \\ 0 & (\theta_1 > \psi_u L) \end{cases} \quad (4)$$

where K_T = torsional rigidity; and θ_1 = relative twist angle about local Axis 1 between the two nodes of a connector element.

Axial Loading and Shear Behavior

Elastic behavior is assumed for shear and axial loading response of the connector beams. The axial stiffness is evaluated by using the assumed dimension of a connector beam, and large shear stiffness is assigned in horizontal direction. The change in axial force ΔN is given as

$$\Delta N = K_N \Delta u_1 = \frac{E_c A_{cr}}{L} \Delta u_1 \quad (5)$$

where K_N = axial stiffness; E_c = Young's modulus of concrete; A_{cr} = area of cracked section; and u_1 = relative axial displacement between the two nodes of a connector element.

The incremental constitutive function for vertical shear V in a connector beam is defined as

$$\Delta V = K_V \Delta u_3 = \left(\frac{L^3}{3E_c I_{cr}} + \frac{6L}{5G_c A_{cr}} \right)^{-1} \Delta u_3 \quad (6)$$

where K_V = shear rigidity; I_{cr} = moment of inertia for cracked beam section about local Axis 2; G_c = shear modulus of concrete; and u_3 = relative vertical displacement between the two nodes of a connector element. Because of the low span-to-depth ratio of a connector beam, the shear stiffness K_V is defined on the basis of the study by Cook et al. (2001) according to Mindlin theory.

An appropriate failure criterion is critical for simulating punching failure and failure propagation. The two-way shear strength defined in ACI 318-11 (ACI 2011) using a nominal shear stress $v_c = 0.33\sqrt{f'_c}$ [in International System of Units (SI)] is not considered. This code provision was developed by excluding the test data of lightly reinforced slab-column connections because their behavior was considered to be controlled by flexure, and the ultimate punching failure was deemed secondary. Because the ACI code formulation does not consider any flexure-shear interaction, it is short of accuracy and often significantly overestimates the strength of lightly reinforced slab-column connections (Tian et al. 2008a). The failure criterion given in the DoD guideline (DoD 2009) correlates punching failure with the inelastic response of slabs. However, the allowable slab plastic deformation was essentially determined from the experimental data of slab-column connections subjected to seismic cyclic lateral loading, in which both the boundary and loading conditions are far different from the column removal scenario.

Accordingly, this study considers Muttoni's formulation (Muttoni 2008), which was established on the basis of a critical crack width theory, to define a punching failure criterion for the connector beams. This formulation, given in Eq. (7), correlates the punching resistance of a slab-column connection with slab local rotation angle. This formulation implies that punching failure is treated as a result of excessive slab flexural deformation localized near the column, and the punching strength decreases as slab rotation capacity increases

$$\frac{V_u}{b_0 d \sqrt{f'_c}} = \frac{3/4}{1 + 15 \frac{\theta_u d}{d_{g0} + d_g}} \text{ (in mm and MPa)} \quad (7)$$

where V_u = connection punching strength; θ_u = slab rotation relative to column at punching failure; d_g = maximum aggregate size; and d_{g0} = reference aggregate size equal to 16 mm. This failure criterion is advantageous because it (1) considers shear-flexure interaction; (2) can be applied to slab-column connections with various punching failure modes regardless of their ductility; and (3) incorporates size effect on shear strength. The punching strength V_u and the failure rotation θ_u in Eq. (7) is implicit because they need to be determined by jointly considering Eq. (7) and the slab shear versus rotation response determined from a nonlinear analysis.

Eq. (7) defines the total shear resistance of an interior slab-column connection under concentric gravity loading. It is assumed

in this study that Eq. (7) can also be used to define punching failure of slab-column connections subjected to unbalanced moments. Because there are two connectors at each side of a column in the proposed macromodel, 1/8 of the shear resistance predicted by Eq. (7) is defined for a connector beam.

Experimental Data for Model Calibration and Validation

The removal of a column in a flat plate results in unevenly distributed bending moment, shear, and torsion at the neighboring slab-column connections where punching failures may occur. To ensure applicability of the proposed macromodel, 24 large-scale experiments of isolated slab-column connections under three different loading conditions (concentric gravity loading, torsion, and uneven gravity loading) are simulated. For all the specimens, quasi-static monotonic loading was applied, no slab shear reinforcement was used, and the maximum aggregate size needed to use Eq. (7) was reported. Table 1 summarizes the geometric and material properties of the test specimens covering a wide range of material properties (concrete compressive strength from 14.2 to 47.4 MPa, steel yield strength from 294 to 570 MPa, and slab tensile reinforcement ratio from 0.25 to 2.00%). Because flat-plate buildings typically have a slab flexural reinforcement ratio of less than 1% (Sherif and Dilger 1996), majority of the selected slab-column specimens are lightly or moderately reinforced to reflect this practice.

Concentric Gravity Loading Tests

Six experiments conducted by Elstner and Hognestad (1956) are simulated. In these tests, as shown in Fig. 7(a), the slabs were inversely placed and supported along four edges. The supports restrained the vertical displacement of slab edges, but the four corners

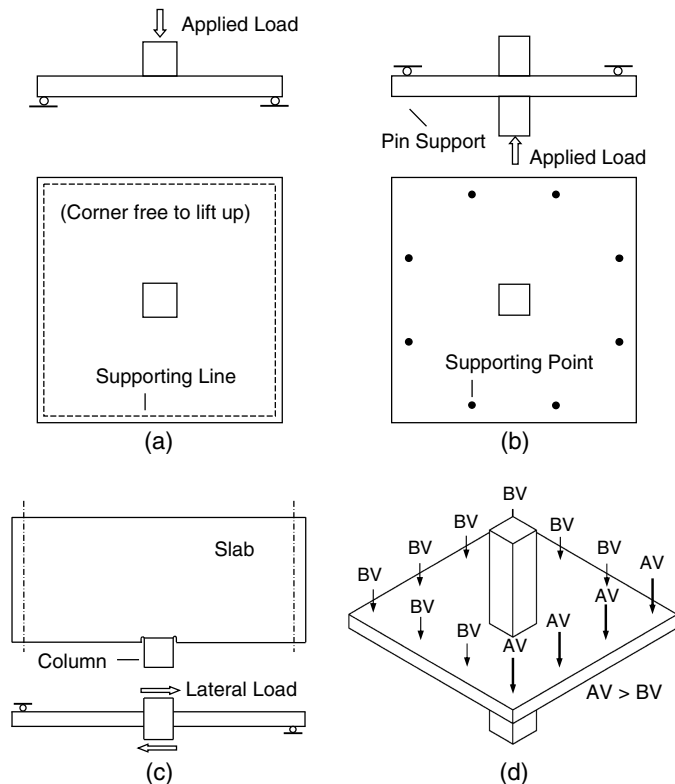


Fig. 7. Test setup for slab-column connections without in-plane restraints

were free to lift up. Downward load was applied on a specimen through the center column stub. The concentric loading tests to be simulated also include four tests conducted by Broms (2000) and Guandalini et al. (2009) using a test setup shown in Fig. 7(b). In each of these tests, a specimen was placed in normal position, an upward load was applied through the center column stub, and the slab vertical displacement was restrained at eight symmetrically distributed points that simulated the location of slab inflection line surrounding a column.

The aforementioned experiments were carried out without applying in-plane restraints to the slabs. Under gravity loading, the slab near the column tends to expand outward. This expansion, however, is restrained by the surrounding portion of slab. Accordingly, compressive membrane action develops in the slab and may increase its punching resistance. In addition to the numerical study presented in this paper, experiments of laterally restrained (Specimens 1.0RE and 0.64RE-NH2 in Table 1) and unrestrained slab-column connections (Specimens 1.0UN and 0.67UN) are conducted in this study. Fig. 8 shows the test setup that permits restraining slab in-plane expansion. The slab of a specimen was connected with eight clevises (two per side) around the slab perimeter that were used to simulate the slab inflection line in a flat-plate building. Each clevis was vertically supported by a steel column (the circular column shown in Fig. 8) and horizontally anchored against a steel section (the rectangular section shown in Fig. 8) that was fixed to the column flange of a steel loading frame. For the tests of slabs without in-plane restraints, the horizontal restraint applied to the clevis was removed. Each slab was subjected to a concentrated load applied downward at the center column stub. Four of this series of experiments are simulated to examine the effectiveness of the proposed model for slabs under compressive membrane action.

Torsional Loading Tests

The unique tests conducted by Kanoh and Yoshizaki (1979) permitted directly identifying the torsional resistance of slab-column connections. As shown in Fig. 7(c), the slab was connected to only one side of the column and roller-supported at two slab edges. The rollers restrained the vertical displacement of slab at its left and right edges. The two other slab edges parallel to loading direction were unrestrained. Torsion transferred from the column stub to the slab was introduced by applying lateral loads in opposite directions on the top and bottom ends of the column stub. Four tests of specimens with varying slab widths and flexural reinforcement ratios are simulated.



Fig. 8. Test setup for slab-column connections subjected to in-plane restraints

Uneven Gravity Loading Tests

Six slab-column specimens tested by Hawkins et al. (1989) are considered. As shown in Fig. 7(d), vertical loads were unequally distributed around slab perimeter, causing unbalanced moment transferred between slab and column. The column of a specimen was anchored with laboratory floor, and the column top end was horizontally restrained. Because of the test boundary condition and the high flexural stiffness of column (as compared with the slab), it can be assumed and verified that the flexural deformation of column caused negligible influence on slab deflection. The level of unbalanced moment was represented by the ratio of unbalanced moment M to the total vertical shear V . For the tests with lower M/V ratio (labeled by AL in Table 1), the vertical loads were maintained so that $AV = 1.49BV$ throughout a test. For the tests with higher M/V ratio (labeled by AH in Table 1), $AV = 6.06BV$. Uneven gravity loading produced not only bending moment and shear but also torsion in slabs, a stress condition similar to that encountered by the neighboring slab-column connections following the removal of a column.

Calibration of Concrete Tension Stiffening Parameters

Concentric gravity loading causes only flexure and shear in slab at the vicinity of column. Thus, the experiments performed on slab-column connections under this simplest loading condition are simulated to calibrate the values of α_1 and α_2 that defining the concrete tension stiffening behavior. To eliminate the effects of using connector elements, the test specimens are modeled by using shell elements only. The material property models for shell elements described previously are applied.

Tension stiffening is influenced by concrete strength and elastic modulus, reinforcement ratio, rebar size and surface condition, and thickness of concrete cover. The studies conducted by Kaklauskas and Ghaboussi (2001) and Stramandinoli and LaRovere (2008) suggested that α_1 generally ranges from 0.1 to 0.6, and α_2 ranges from 5 to 25. For a typical floor slab constructed with normal strength concrete and reinforcing steel and designed following the code-specified detailing requirements for concrete cover and rebar spacing, the values of α_1 and α_2 fall into narrower ranges.

Because of the significant difference in concrete strength and reinforcement ratio, Specimens B-1 and B-4 in Table 1 are used as benchmark to calibrate the appropriate values of α_1 and α_2 . It is found that the FE simulation of a slab-column connection is sensitive to the definitions of concrete tensile stiffening behavior. Fig. 9 shows as example the effects of α_1 and α_2 on the load-center deflection response of these specimens. In Figs. 10(a and b), α_2 is equal to 20 whereas α_1 is defined as 0.2, 0.3, and 0.4. In Figs. 10(c and d), α_1 is fixed at 0.2, but α_2 has different values of 10, 20, and 30. From the calibrations and to obtain better convergence in the numerical analyses, $\alpha_1 = 0.2$ and $\alpha_2 = 20$ are chosen and consistently used in this study to model slab-column connections.

Simulations of Slab-Column Connections Using Shell Elements Only

The calibrated tension stiffening model and other material property models described previously are applied to some experiments listed in Table 1. Only shell elements are used for the numerical simulations. The concentric gravity loading tests conducted by Broms (2000) and Guandalini et al. (2009) are simulated. As shown in

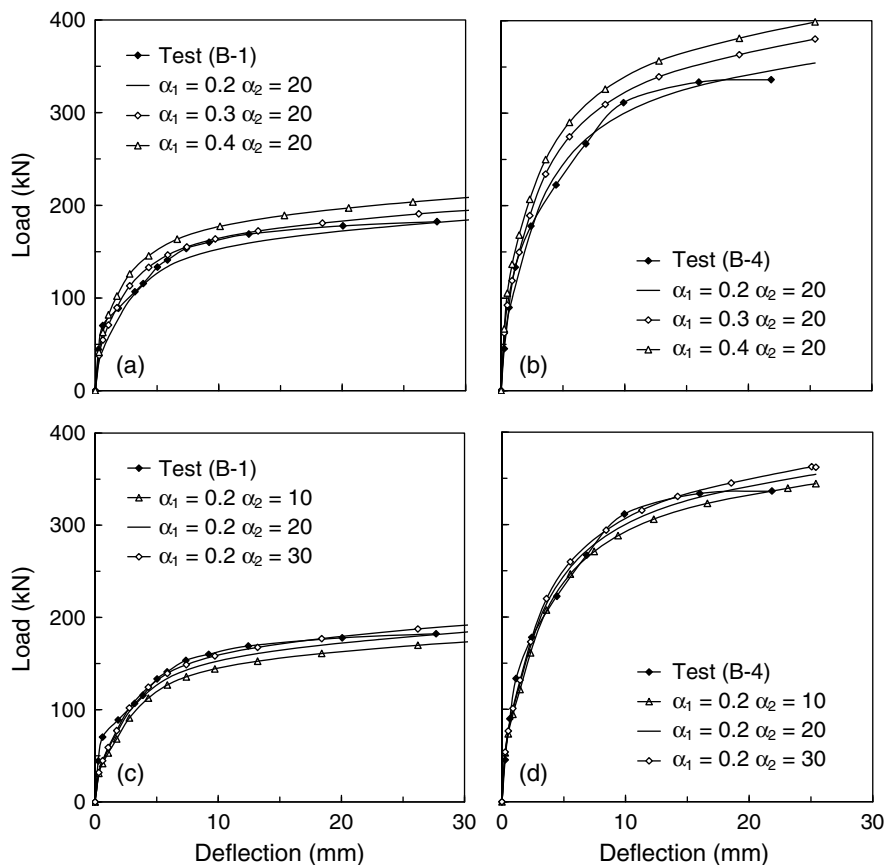


Fig. 9. Effects of concrete tension stiffening parameters on load-deflection response of specimens under concentric gravity loading tested by Elstner and Hognestad (1956)

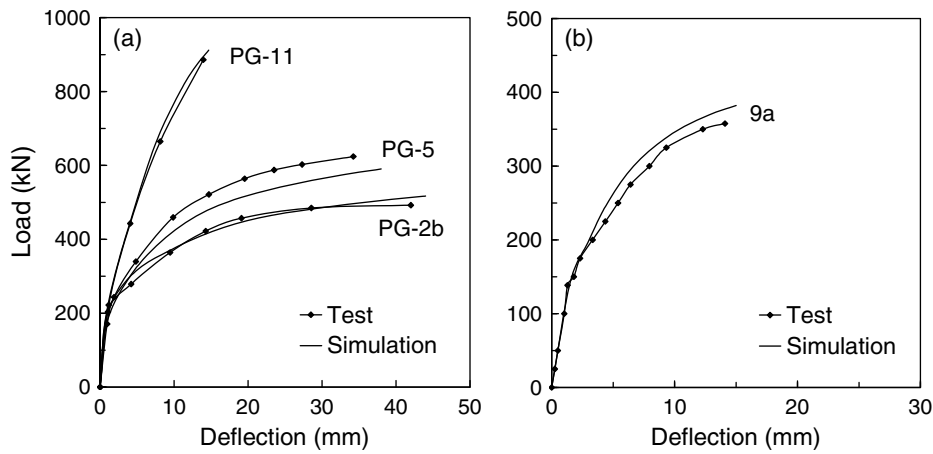


Fig. 10. Load-deflection response predicted by using shell elements only versus test results from Guandalini et al. (2009) and Broms (2000) for specimens under concentric gravity loading

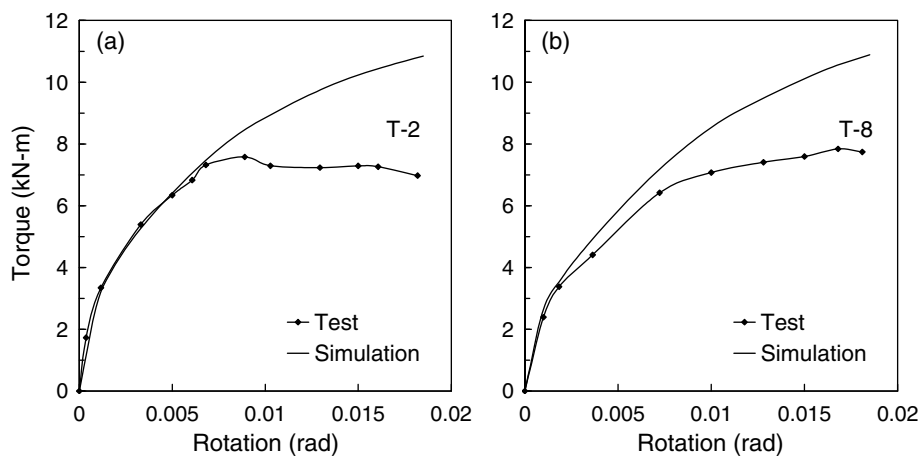


Fig. 11. Torque-twist angle response predicted by using shell elements only versus result of experiments conducted by Kanoh and Yoshizaki (1979)

Fig. 10, using shell elements with calibrated concrete tensile behavior for slabs can reasonably predict the overall load-deflection responses of slab-column connections under symmetric loading condition.

The use of shell element alone is extended to modeling the torsional behavior of slab-column connections. Two torsional loading tests, T-2 and T-1 (Kanoh and Yoshizaki 1979) in Table 1, are simulated. These specimens had identical slab width but different flexural reinforcement ratios. The column stub in the tests was modeled by using rigid shell elements. At the center node of these elements, a torque is applied, and the calculated twist angle is obtained. Fig. 11 compares the measured and the simulated torque versus twist angle response. Fig. 11 shows that good predictions of connection torsional behavior are obtained in the early loading stage; however, likely caused by the constant shear stiffness assumed for shell elements, the torsional stiffness is considerably overestimated beyond a joint rotation of 0.007 rad.

The overestimation of torsional resistance by using shell elements can be further evidenced by simulating slab-column connections subjected to unevenly distributed gravity loads, which causes not only shear and bending moment but also torsion in slab near the column. Four tests in Table 1 conducted by Hawkins et al. (1989) are simulated. The measured and predicted load-deflection responses are compared in Fig. 12, where load refers to the total gravity shear transferred from slab to column, and deflection refers to

that at the midpoint of the slab edge where the heavier loads (AV) shown in Fig. 7(d) were applied. As demonstrated in these figures, the specimens exhibit higher stiffness in simulations than in the experiments because of the overestimated torsional resistance. This indicates that caution needs to be exercised when using shell elements to simulate the response of slab-column connections transferring unbalanced moments.

Validation of Proposed Macromodel

The proposed macromodel is applied to all the experiments given in Table 1. Identical modeling approach for material properties is used to define the shell elements that simulate the slabs outside the assumed punching perimeter. The behavioral models for flexure, torsion, and shear and the failure criterion for connector beams are incorporated.

Concentric Gravity Loading

The 10 experiments in Table 1 conducted under concentric gravity are simulated by performing displacement-driven analyses until the predefined punching failure condition is recognized at the connector beams. For the tests of 1.0RE and 0.67RE-NH, in which in-plane restraints were applied, two elastic spring elements are

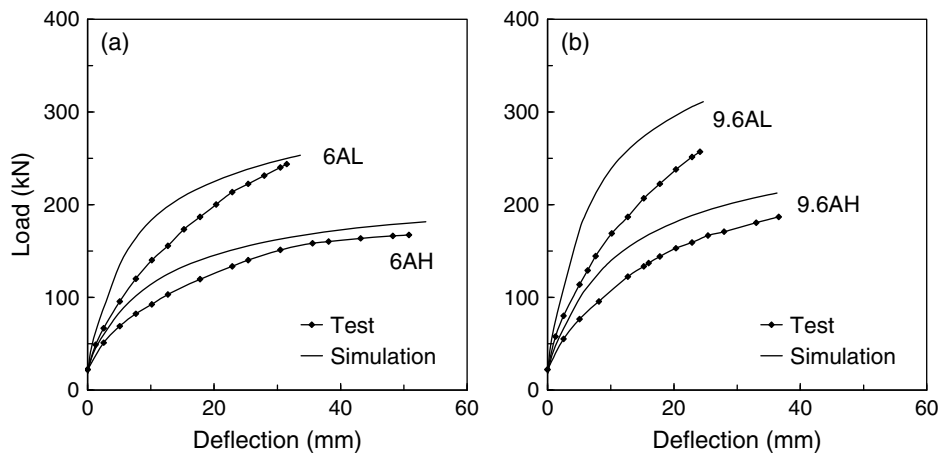


Fig. 12. Load-deflection response predicted by using shell elements only versus test results from Hawkins et al. (1989) for specimens subjected to uneven gravity loading

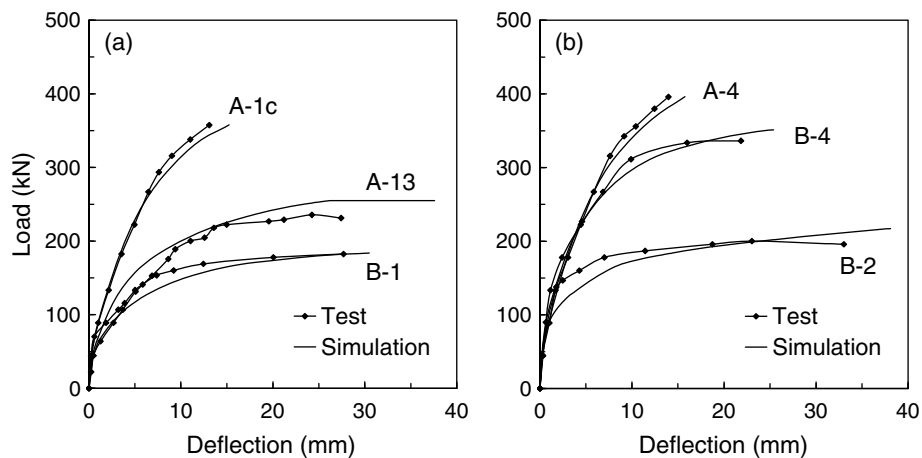


Fig. 13. Load-deflection response predicted by using proposed macromodel versus test results from Elstner and Hognestad (1956) for specimens under concentric gravity loading

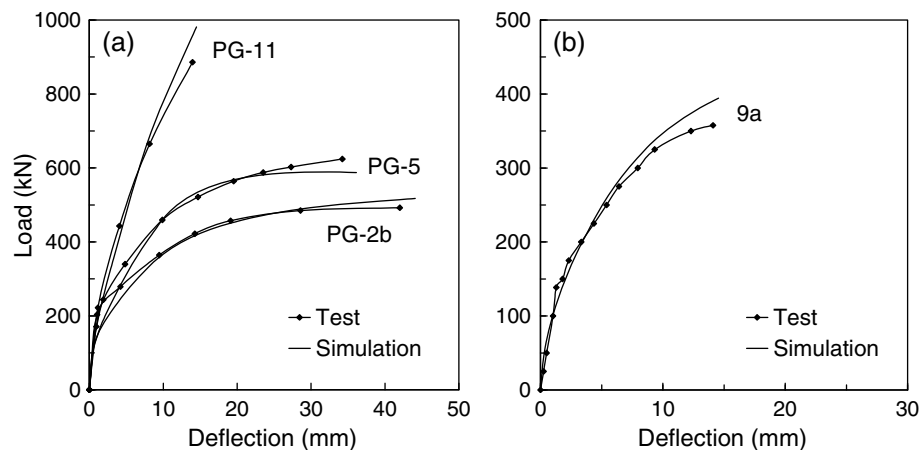


Fig. 14. Load-deflection response predicted by using proposed macromodel versus test results from Guadalini et al. (2009) and Broms (2000) for specimens under concentric gravity loading

connected with the shell elements at each edge of the slab. Each spring, having an axial stiffness defined according to measured test data regarding the rigidity of lateral restraint, is situated in the plane of slab and perpendicular to slab edge.

The simulated load-deflection response is presented in Figs. 13–15, in which the ending point of a curve corresponds to the punching failure identified from the test or the FE analysis. Once the failure is detected in a simulation at one side of a

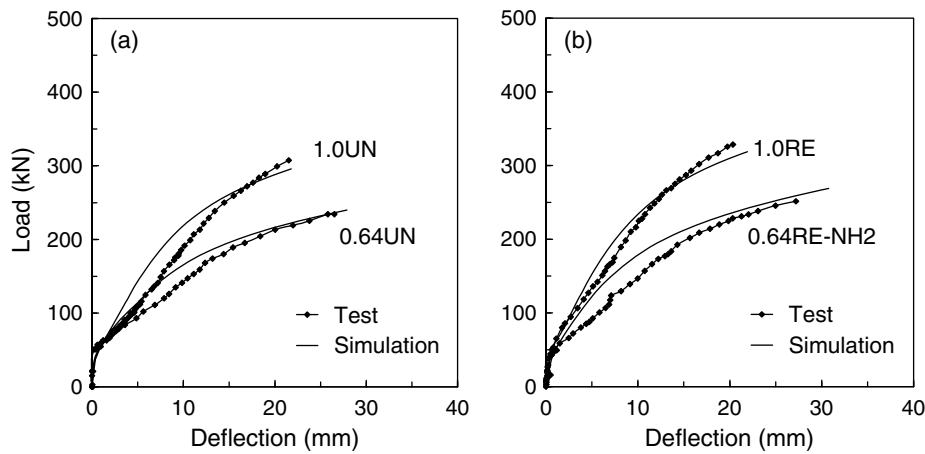


Fig. 15. Load-deflection response predicted by using proposed macromodel versus result for specimens tested in this study under concentric gravity loading

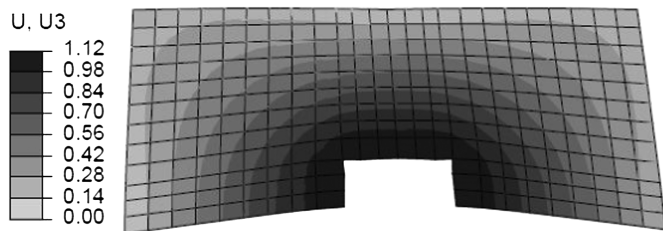


Fig. 16. Deformation shape of Specimen B-2 using proposed macromodel (unit: in.; 1 in. = 25.4 mm)

slab-column connection, the loading capacity at this side immediately drops down to zero through the separation of connector beam from slab. Likely caused by the variability in both the actual and modeled concrete tensile properties, some discrepancies exist between the measured and calculated postcracking stiffness. However, in terms of the overall nonlinear response and the ultimate loading capacity, the predicted and measured load-deflection responses of the test specimens generally agree well. Moreover, except for Specimen A-13, the ultimate deformation capacity of a slab-column is well captured by the failure criterion adopted in this study. Fig. 16 shows the deformation shape of half of Specimen B-2 before its punching failure. It is seen that slab plastic deformation is concentrated near the critical section, and the centerline of the slab rotates about the critical section as a rigid body, a behavior consistent with the observation made from experiments conducted by Guandalini et al. (2009).

Using shell elements alone and jointly using shell and connector elements lead to very similar load-deformation response, as shown by comparing Figs. 10 and 14 for the simulated behaviors of Specimens PG-11, PG-5, PG2-B, and 9a. This can partially validate the uncoupled flexure and shear for the short connector elements and the constitutive models for these two actions. The effectiveness of the suggested model is also examined by the yielding pattern of slabs. Fig. 17 shows the predicted force in rebar oriented in two orthogonal directions for Specimen B-2. The rebar yielding force is evaluated according to the reported material property and layout of reinforcing bars. The gray color corresponding to force greater than 40.6 kN (9,340 lbF) denotes the yielded zone of slab. The dashed lines show the yield-line pattern derived from Johansen's yield-line theory (Elstner and Hognestad 1956) corresponding to

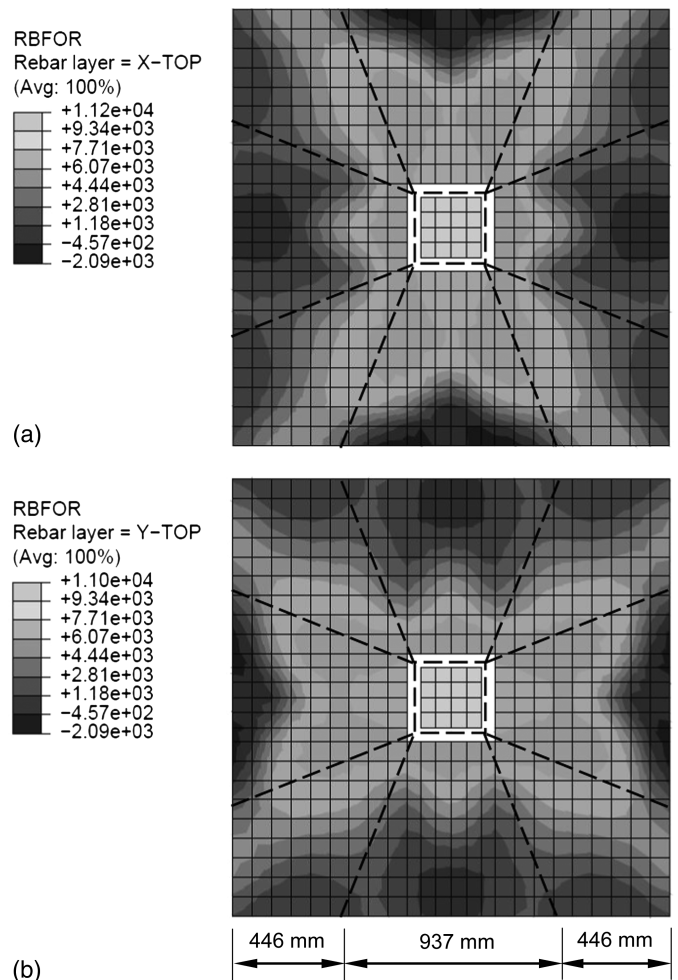


Fig. 17. Rebar forces of slab top reinforcement for Specimen B-2 (unit for rebar force: lbF; 1 lbF = 4.45 N): (a) in X -direction; (b) in Y -direction

the test boundary condition. The yield-lines consist of those developed at slab-column interface during the early loading stage and those extending from column corners to slab edges later. Overlapping Figs. 17(a and b) indicates that, even though the use of

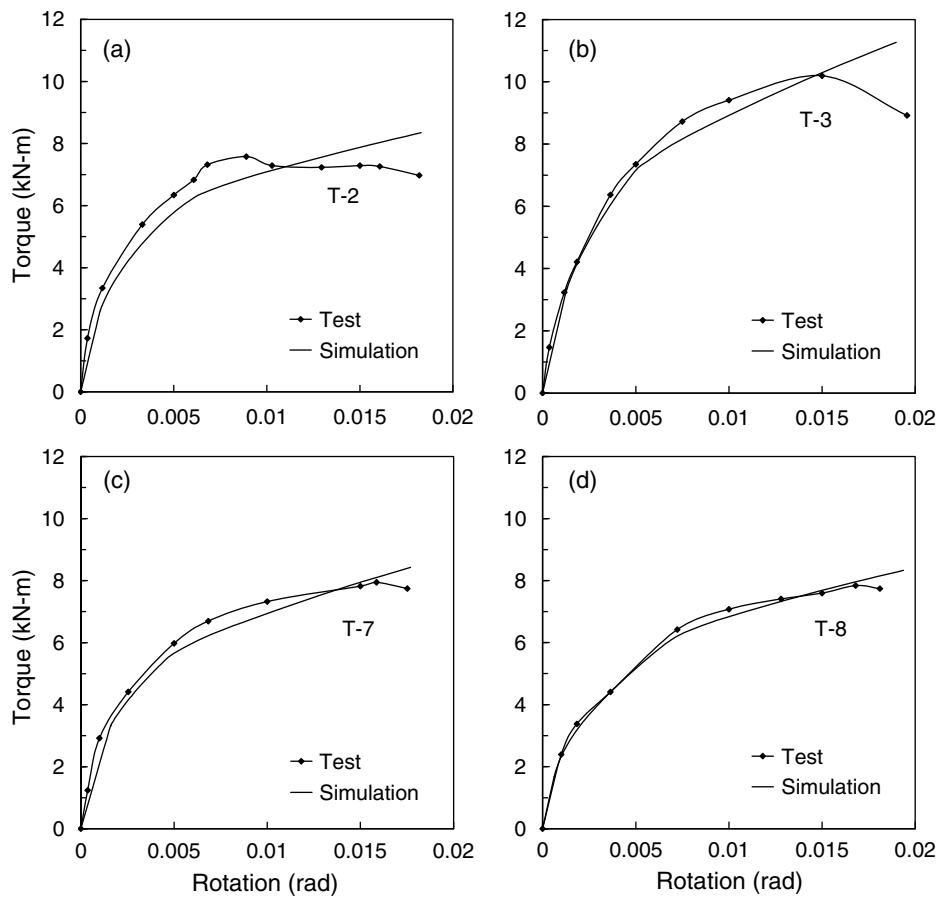


Fig. 18. Torque-twist angle response predicted by using proposed macromodel versus result of experiments conducted by Kanoh and Yoshizaki (1979)

connector beams causes discontinuity in element types at critical section, the predicted yielding pattern determined from analysis is consistent with the theoretical yield lines.

Torsional Loading

The proposed macromodel is applied to four torsional loading tests conducted by Kanoh and Yoshizaki (1979), in which the external loads caused mainly torsion in the slab neighboring column. Because it is assumed that torsion does not cause a punching failure, the failure criterion is not considered for the connector beam elements. Fig. 18 compares the predicted torque versus twist angle response with the test result. It is seen that the measured behavior of the specimens in terms of stiffness degradation and strength can be well simulated by the macromodel. Given that slab outside the direct vicinity of column mainly resists bending, which can be appropriately simulated by shell elements, the adequacy of torsional stiffness and strength of connector beams defined by Eqs. (2) and (3) is verified. At a connector beam, both torsion and vertical shear provide torsional resistance. Because a linear elastic behavior is assumed for shear in the connector beams, the overall response does not have a yield plateau.

Uneven Gravity Loading

Force-driven analyses are conducted on the six slab-column connections tested under unevenly distributed gravity loads (Hawkins et al. 1989). Loading is applied in the analysis of a specimen until the shear versus slab rotation response at the heavily loaded side of

slab meets the punching failure criterion. Fig. 19 compares the calculated and measured load-deflection response of the specimens. Comparisons can be made on stiffness, strength, and deformation capacity. As Fig. 19 shows, the loading capacity of all specimens is accurately predicted by numerical simulations using the macromodel. Except for Specimens 9.6AL and 14AH, the stiffness degradation during loading is also well predicted. It appears that the stiffness of Specimen 14AH is well overestimated. However, before reaching a load of approximately 140 kN, the load-deformation response of this specimen was reported to be almost identical to that of Specimen 9.6AH. Should 14AH exhibit in the test higher postcracking stiffness than 9.6AH because of the almost same concrete strength but much higher reinforcement ratio, the predicted response would have been closer to the test result.

The good accuracy of predicting loading capacity by using the proposed macromodel can be attributed to not only the appropriateness of using shell elements to simulate the flexural behavior of slab but also the effectiveness of the torsional resistance model defined for the connector beams. The analysis results obtained from the connector beams indicate that, for specimens labeled with AH (carrying higher levels of unbalanced moment), a significant portion of load-carrying capacity is provided by torsion. For instance, it is found that torsion at the connection side faces of Specimen 6AH resists up to 42% of the total unbalanced moment transferred between slab and column. This highlights the significance of appropriately modeling the torsional behavior of a slab-column connection subjected to unbalance moment.

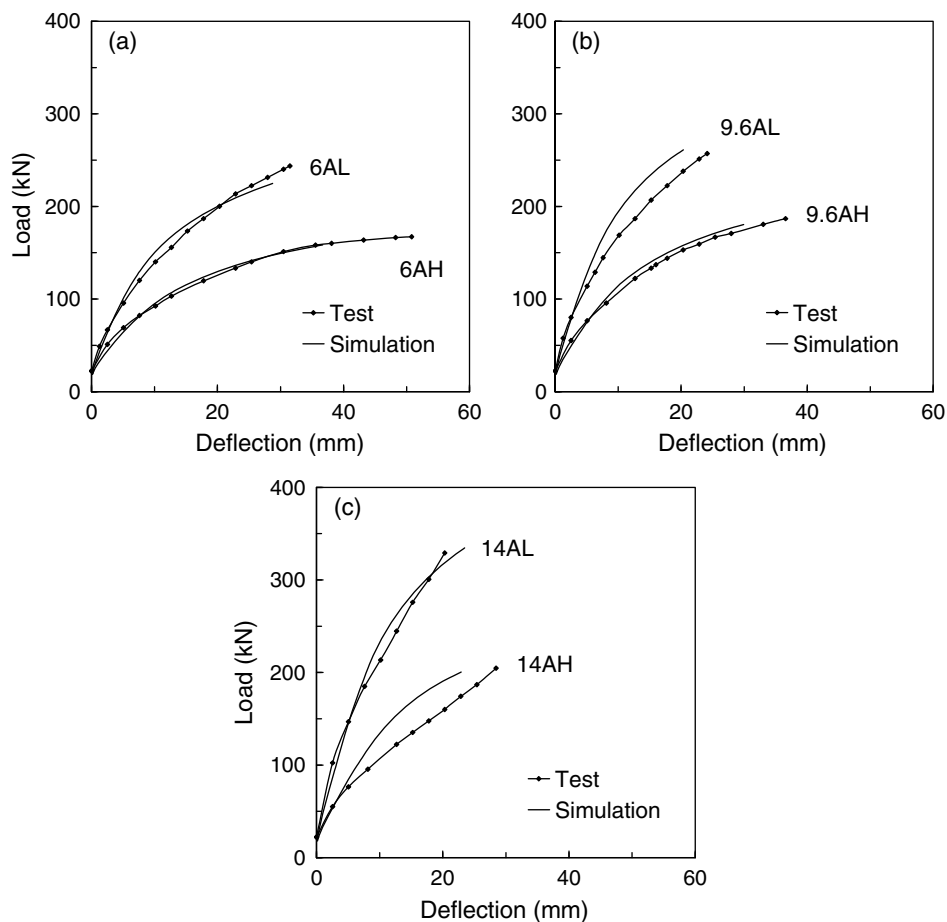


Fig. 19. Load-deflection response predicted by using proposed macromodel versus test results from Hawkins et al. (1989) for specimens subjected to uneven gravity loading

Summary and Conclusions

This study develops a macromodel for use in the progressive collapse analyses of reinforced concrete flat-plate structures. The model, which jointly uses thin shell elements and connector beam elements, is capable of simulating the nonlinear behavior of slab-column connections under complex loading conditions. The shell elements embedded with rebar layer simulate the flexural behavior of slabs. The connector beam elements defined with nonlinear response for primary bending and torsion and with a deformation-based punching failure criterion are used to transfer forces from slab to column, detect punching failure, and enable the separation of slab from column on a punching failure. Two parameters defining concrete tension stiffening property of slab concrete are calibrated from using shell elements to simulate two tests under concentric gravity loading. Other modeling parameters are defined on the basis of available information in literature. The proposed macromodel, which jointly uses shell and connector elements, is validated by 24 large-scale tests of isolated slab-column connections under a wide range of loading conditions, including concentric gravity loading with and without in-plane restraint, pure torsion, and unevenly distributed gravity loading.

For slab-column connections under concentric gravity loading, using shell elements can predict accurately the load-deflection response of slab-column connections. However, likely because of assuming a constant concrete shear stiffness, the use of shell elements alone results in a significant overestimated torsional resistance of slab-column connections. Such a deficiency leads to overestimated

stiffness and strength of slab-column connections transferring unbalanced moment caused by unevenly distributed gravity loads.

This study verifies the suggested macromodel on the basis of the data of static loading tests conducted on isolated interior slab-columns. The applicability of this model needs to be further examined for slab-column connections having columns with rectangular cross section, slab-column connections subjected to higher loading rates, and corner and exterior slab-column connections in which the response can be dominated by torsion. In addition, the punching failure criterion adopted in this study was developed by Muttoni (2008) by using test data of slab-column connections under concentric gravity loading. Further validations of this failure criterion should be made for slab-column connections under more complex loading conditions. It is likely that using more connector elements at each side of slab-column interface or considering coupled behavior among different actions in the connectors, especially torsion and flexure, can enhance the proposed model. Future studies are also suggested to improve the modeling of connector beam elements so that the post-punching resistance slabs with and without continuous slab bottom reinforcement at columns can be simulated more precisely.

Acknowledgments

This paper is based on work supported by the National Science Foundation under Grant Nos. 1100877 and 1100146. The authors gratefully acknowledge the financial support from the National

Science Foundation. The opinions, findings, and conclusions or recommendations expressed in this paper are those of the authors and do not necessarily reflect the views of the sponsor.

References

- ABAQUS 6.10 [Computer software]. Waltham, MA, Dassault Systèmes.
- ACI (American Concrete Institute). (2011). "Building code requirements for structural concrete and commentary." *ACI 318-11*, Farmington Hills, MI.
- Akiyama, H., and Hawkins, N. M. (1984). "Response of flat plate concrete structures to seismic and wind forces." *Structures and Mechanics Rep. SM84-1*, Univ. of Washington, WA.
- Bao, Y., Kunnath, S. K., El-Tawil, S., and Lew, H. S. (2008). "Macromodel-based simulation of progressive collapse: RC frame structures." *J. Struct. Eng.*, 10.1061/(ASCE)0733-9445(2008)134:7(1079), 1079–1091.
- Broms, C. E. (2000). "Elimination of flat plate punching failure mode." *ACI Struct. J.*, 97(1), 94–101.
- Cook, R. D., Malkus, D. S., Plesha, M. E., and Witt, R. J. (2001). *Concept and applications of finite element analysis*, 4th Ed., Wiley, New York.
- Coronelli, D. (2010). "Grid model for flat-slab structures." *ACI Struct. J.*, 107(6), 645–653.
- Criswell, M. E. (1974). "Static and dynamic response of reinforced concrete slab-column connections." *ACI Special Publication*, 42-31, 721–746.
- DoD (Department of Defense). (2009). "Design of building to resist progressive collapse." *Unified Facility Criteria (UFC) 4-023-03*, Washington, DC.
- Elstner, R. C., and Hognestad, E. (1956). "Shearing strength of reinforced concrete slabs." *ACI J.*, 53(1), 29–58.
- Gardner, N. J., and Shao, X. (1996). "Punching shear of continuous flat reinforced concrete slabs." *ACI Struct. J.*, 93(2), 218–228.
- Guandalini, S., Burdet, O. L., and Muttoni, A. (2009). "Punching tests of slabs with low reinforcement ratios." *ACI Struct. J.*, 106(1), 87–95.
- Hawkins, N. M., Bao, A. B., and Yamazaki, J. (1989). "Moment transfer from concrete slabs to columns." *ACI Struct. J.*, 86(6), 705–716.
- Hognestad, E. (1951). "A study of combined bending and axial load in reinforced concrete members." *Bulletin Series No. 399*, Univ. of Illinois Engineering Experimental Station.
- Hsu, T. T. C. (1968a). "Torsion of structural concrete-behavior of reinforced concrete rectangular members." *ACI Special Publication*, 18-08, 261–306.
- Hsu, T. T. C. (1968b). "Torsion of structural concrete-plain concrete rectangular sections." *ACI Special Publication*, 18-10, 203–238.
- Kaklauskas, G., and Ghaboussi, J. (2001). "Stress-strain relations for cracked tensile concrete from RC beam tests." *J. Struct. Eng.*, 10.1061/(ASCE)0733-9445(2001)127:1(64), 64–73.
- Kang, T. H.-K., Wallace, J. W., and Elwood, K. J. (2009). "Nonlinear modeling of flat-plate systems." *J. Struct. Eng.*, 10.1061/(ASCE)0733-9445(2009)135:2(147), 147–158.
- Kanoh, Y., and Yoshizaki, S. (1979). "Strength of slab-column connections transferring shear and moment." *ACI Struct. J.*, 76(2), 461–478.
- Khandelwal, K., El-Tawil, S., Kunnath, S. K., and Lew, H. S. (2008). "Macromodel-based simulation of progressive collapse: Steel frame structures." *J. Struct. Eng.*, 10.1061/(ASCE)0733-9445(2008)134:7(1070), 1070–1078.
- Lee, J., and Fenves, G. L. (1998). "Plastic-damage model for cyclic loading of concrete structures." *J. Eng. Mech.*, 10.1061/(ASCE)0733-9399(1998)124:8(892), 892–900.
- Lips, S., Ruiz, M. F., and Muttoni, A. (2012). "Experimental investigation on punching strength and deformation capacity of shear-reinforced slabs." *ACI Struct. J.*, 109(6), 889–900.
- Loo, Y.-C., and Guan, H. (1997). "Cracking and punching shear failure analysis of RC flat plates." *J. Struct. Eng.*, 10.1061/(ASCE)0733-9445(1997)123:10(1321), 1321–1330.
- Lubliner, J., Oliver, J., Oller, S., and Oñate, E. (1989). "A plastic-damage model for concrete." *Int. J. Solids Struct.*, 25(3), 299–326.
- Luo, Y. H., Durrani, A. J., and Conte, J. P. (1995). "Equivalent frame analysis of flat plate buildings for seismic loading." *J. Struct. Eng.*, 10.1061/(ASCE)0733-9445(1994)120:7(2137), 2137–2155.
- Marzouk, H. M., and Chen, Z. (1993). "Finite element analysis of high-strength concrete slabs." *ACI Mater. J.*, 90(5), 505–513.
- Massicotte, B., Elwi, A. E., and MacGregor, J. G. (1990). "Tension stiffening model for planar reinforced concrete members." *J. Struct. Eng.*, 10.1061/(ASCE)0733-9445(1990)116:11(3039), 3039–3058.
- Mercan, B., Schultz, A. E., and Stolarski, H. K. (2010). "Finite element modeling of prestressed concrete spandrel beams." *Eng. Struct.*, 32(9), 2804–2813.
- Moe, J. (1961). "Shearing strength of reinforced concrete slabs and footings under concentrated loads." *Development Dept. Bulletin No. D47*, Portland Cement Association, Skokie, IL.
- Morrison, D. G., Hirasawa, I., and Sozen, M. A. (1983). "Lateral-load tests of R/C slab-column connections." *J. Struct. Eng.*, 10.1061/(ASCE)0733-9445(1983)109:11(2698), 2698–2714.
- Muttoni, A. (2008). "Punching shear strength of reinforced concrete slabs without transverse reinforcement." *ACI Struct. J.*, 105(4), 440–450.
- Parisch, H. (1979). "A critical survey of the 9-node degenerated shell element with special emphasis on thin shell application and reduced integration." *Comput. Meth. Appl. Mech. Eng.*, 20(3), 323–350.
- Polak, M. A. (1998). "Modeling punching shear of reinforced concrete slabs using layered finite elements." *ACI Struct. J.*, 95(1), 71–80.
- Robertson, I. N. (1997). "Analysis of flat slab structures subjected to combined lateral and gravity loads." *ACI Struct. J.*, 94(6), 723–729.
- Sherif, A. G., and Dilger, W. H. (1996). "Critical review of the CSA A23.3-94 punching shear strength provisions for interior columns." *Can. J. Civ. Eng.*, 23(5), 998–1011.
- Sheu, M. S., and Hawkins, N. M. (1980). "Grid model for predicting the monotonic and hysteretic behavior of slab-column connections transferring moments." *ACI Special Publication*, 63-04, 79–111.
- Stramandinoli, R. S. B., and LaRovere, H. L. (2008). "An efficient tension-stiffening model for nonlinear analysis of reinforced concrete members." *Eng. Struct.*, 30(7), 2069–2080.
- Tian, Y. (2007). "Behavior and modeling of reinforced concrete slab-column connections." Ph.D. dissertation, Univ. of Texas at Austin, Austin, TX.
- Tian, Y., Chen, J., Said, A., and Zhao, J. (2012). "Nonlinear modeling of flat-plate structures using grid beam elements." *Comput. Concr.*, 10(5), 489–505.
- Tian, Y., Jirsa, J. O., and Bayrak, O. (2008a). "Strength evaluation of interior slab-column connections." *ACI Struct. J.*, 105(6), 692–700.
- Tian, Y., Jirsa, J. O., and Bayrak, O. (2009). "Nonlinear modeling of slab-column connections under cyclic loading." *ACI Struct. J.*, 106(1), 30–38.
- Tian, Y., Jirsa, J. O., Bayrak, O., Widiyanto, and Argudo, J. F. (2008b). "Behavior of slab-column connections of existing flat-plate structures." *ACI Struct. J.*, 105(5), 561–569.
- Wang, W., and Teng, S. (2008). "Finite-element analysis of reinforced concrete flat plate structures by layered shell element." *J. Struct. Eng.*, 10.1061/(ASCE)0733-9445(2008)134:12(1862), 1862–1872.